A New Sliding Mode Control Proposal with a Clegg Integrator for a Mobile Manipulator

Pablo Proaño[®]a, Paulo Leica[®]b and Gabriela Andaluz[®]c

Escuela Politécnica Nacional, Departamento de Automatizacion y Control Industrial, Quito, Ecuador

Keywords: Mobile Manipulator, Sliding Mode Control, Clegg Integrator, Trajectory Tracking, Discontinuous Control,

Chattering Reduction, Nonlinear Control.

Abstract: This article presents a novel control strategy for trajectory tracking in mobile manipulators. The proposed

method combines a conventional Sliding Mode Controller (SMC) with a reset-based integrator, specifically a Clegg integrator, applied to the discontinuous component of the sliding surface. The system under study consists of a mobile platform with dynamic behavior and a robotic arm modeled kinematically. The main objective is to improve tracking performance and reduce control signal oscillations, particularly under abrupt reference changes and external disturbances. A reference trajectory with an inclined square shape is used to challenge the controller with sudden directional transitions. To evaluate the effectiveness of the proposed approach, both the classical SMC and the SMC+Clegg controllers are implemented and tested under the same conditions. The performance is analyzed using standard indices such as Integral Square Error (ISE), Integral Absolute Error (IAE), and Total Variation of the control signal (TVu). Results show that the proposed controller achieves improved trajectory tracking with reduced overshoot and chattering, while maintaining robustness to disturbances. Stability is formally demonstrated using Lyapunov theory. The positive impact of the Clegg integrator is highlighted in the discontinuous control component, allowing for reduced control effort

without compromising tracking quality or disturbance rejection.

SCIENCE AND TECHNOLOGY PUBLICATIONS

1 INTRODUCTION

The modeling of mobile manipulators is commonly performed using state-space representations, where inverse Jacobian matrices are employed to compute the joint velocities required to follow a desired endeffector trajectory. Since the mobile platform typically has greater mass than the robotic arm, a dynamic model is used for the base and a kinematic model for the manipulator to simplify the formulation while preserving accuracy (Haddadin et al., 2022; Widhiada et al., 2020; Delgado et al., 2022). Reference trajectories with abrupt changes are often applied to test the robustness and reactivity of controllers under demanding conditions (You et al., 2019; Kemp et al., 2022).

A wide range of control techniques has been proposed for mobile manipulators, including PID, null-space optimization, fuzzy logic, and sliding mode control (SMC) (Salinas et al., 2018; Moreno et al.,

ap https://orcid.org/0000-0002-6902-7151

^b https://orcid.org/0000-0002-5385-1920

co https://orcid.org/0000-0002-1822-6943

2021). More recently, hybrid control approaches have been explored to improve interaction performance and adaptability, incorporating learning-based impedance tuning (Zhao et al., 2022) and coordinated actuation mechanisms (Gan et al., 2022). PID controllers are extensively used in industry due to their simplicity and effectiveness, although in robotic applications they are often embedded into hybrid strategies (Zangina et al., 2020; Maung et al., 2024). A key limitation of PID controllers lies in the integral windup phenomenon, which can degrade system performance by introducing overshoots and increasing settling times (Hitit et al., 2023; Okelola et al., 2020; Chaudhary, 2024).

Reset-based techniques have emerged to address this issue. One notable solution is the Clegg integrator (CI), a nonlinear integrator that resets its state when the error derivative crosses zero. The CI reduces the accumulation of the integral term, thereby limiting overshoot and improving transient performance (Beerens et al., 2022; Gholipour et al., 2015; Kolar and Lazar, 2021). Recent developments have extended this concept through soft-reset con-

trollers, which approximate hard-reset behavior using continuous-time differential inclusions. These controllers preserve passivity properties and offer improved stability guarantees under convex Lyapunov conditions, facilitating their application in robotic systems (Le and Teel, 2021; Teel, 2022). In recent work by Proaño et al. (Proaño et al., 2024), the use of a Clegg integrator in a PID-type sliding surface demonstrated faster settling, reduced chattering, and improved overall performance compared to conventional SMC and PID strategies. The reset action was shown to affect only the discontinuous component of the SMC, resulting in a smoother control signal without compromising the system's robustness.

Sliding Mode Control remains a robust strategy for handling modeling uncertainties and external disturbances. It consists of a continuous term that maintains system convergence on the sliding surface and a discontinuous term responsible for driving the state toward it. The latter, however, tends to introduce high-frequency oscillations, or chattering, which several studies have sought to mitigate using smoothed switching functions and hybrid surfaces (Gude et al., 2024; Demim et al., 2023; Li et al., 2024). Recent advancements have further explored chattering reduction through higher-order and adaptive SMC strategies (V and Manthati, 2024), as well as the use of chattering-attenuation disturbance observers (CADOB), which effectively suppress highfrequency components in the disturbance estimation without degrading control performance (Yim et al., 2023).

This paper proposes a sliding mode control strategy that incorporates a Clegg-type integrator into the sliding surface. The reset action aims to mitigate windup, reduce overshoot, and improve settling time. The controller is implemented on a mobile manipulator and evaluated under setpoint changes and external disturbances. Performance indices are calculated to compare the proposed method with conventional strategies. The main contributions include improved response time, reduced overshoot, enhanced recovery from disturbances, and ease of implementation in systems that already use PID architectures.

2 MOBILE MANIPULATOR MODEL

Before implementing the proposed control strategies, it is essential to understand the structure and behavior of the mobile manipulator. This system consists of a mobile platform, modeled using a dynamic approach, and a robotic arm, described through a kinematic

model. This section presents both models, which enable an accurate representation of the system's evolution in response to control signals and reference trajectories.

A graphical representation of the mobile manipulator used in the present work is shown in Figure 1.

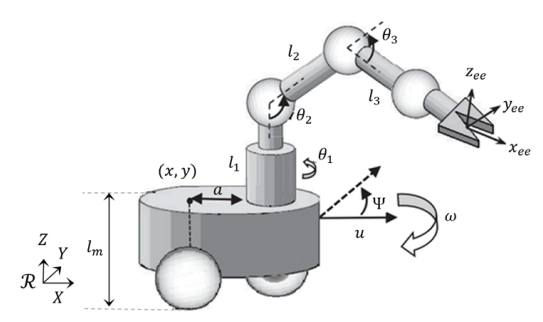


Figure 1: Mobile manipulator with three degrees of freedom, (Vizuete et al., 2017).

Where l_m represents the vertical distance from the ground to the base of link 1 of the manipulator; l_1 , l_2 , and l_3 are the lengths of the manipulator links; a denotes a point of interest introduced to eliminate the non-holonomic constraint; and b is the distance from the center of the mobile platform to link 1. The parameter a has no physical structure but is geometrically defined to lift the non-holonomic restriction of the platform's motion model. The variables θ_1 , θ_2 , and θ_3 correspond to the rotation angles of links l_1 , l_2 , and l_3 , respectively. The coordinates x and y represent the position of the mobile robot's base, and ψ denotes its orientation, while u and ω represent the linear and angular velocities of the mobile platform, respectively. Finally, x_{ee} , y_{ee} , and z_{ee} define the position of the end-effector with respect to the origin of the coordinate system.

The position of the end-effector (x_{ee}, y_{ee}, z_{ee}) as a function of the system's angles and parameters is computed using the following expressions:

$$x_{ee} = x + b\cos(\psi) + \cos(\theta_1 + \psi) (l_2\cos(\theta_2) + l_3\cos(\theta_2 + \theta_3))$$
(1)

$$y_{ee} = y + b\sin(\psi) + \sin(\theta_1 + \psi) (l_2\cos(\theta_2) + l_3\cos(\theta_2 + \theta_3))$$
(2)

$$z_{ee} = l_1 + l_m + l_2 \sin(\theta_2) + l_3 \sin(\theta_2 + \theta_3)$$
 (3)

The kinematic behavior of the mobile platform is described by the following equations:

$$\dot{x} = u\cos\psi - a\omega\sin\psi \tag{4}$$

$$\dot{\mathbf{y}} = u\sin\mathbf{\Psi} + a\mathbf{\omega}\cos\mathbf{\Psi} \tag{5}$$

$$\dot{\Psi} = \omega \tag{6}$$

Where x and y denote the position of the mobile robot base, and ψ represents its orientation. The variable u corresponds to the linear velocity of the mobile platform, while ω denotes its angular velocity.

The kinematics of the mobile manipulator h is determined by:

$$\dot{h}_{ee} = J_{ee} \, \dot{q} \tag{7}$$

Where J_{ee} is the Jacobian matrix that relates the

generalized velocities $\dot{q} = [u, \omega, \dot{\theta}_1, \dot{\theta}_2, \dot{\theta}_3]^T$ to the Cartesian velocity of the end-effector. The vector $h_{ee} = [x_{ee}, y_{ee}, z_{ee}]^T$ represents the Cartesian position of the end-effector in the task space, and is used to describe its spatial motion relative to the global coordinate system.

The Jacobian matrix J_{ee} , using the trigonometric shorthand defined in the implementation, is given by:

$$J_{ee} = \begin{bmatrix} C_{\Psi} & -aS_{\Psi} - bS_{\Psi} - S_{\theta_1 \Psi}(l_2 C_{\theta_2} + l_3 C_{\theta_2 \theta_3}) & -S_{\theta_1 \Psi}(l_2 C_{\theta_2} + l_3 C_{\theta_2 \theta_3}) & -C_{\theta_1 \Psi}(l_2 S_{\theta_2} + l_3 S_{\theta_2 \theta_3}) & -l_3 C_{\theta_1 \Psi} S_{\theta_2 \theta_3} \\ S_{\Psi} & aC_{\Psi} + bC_{\Psi} + C_{\theta_1 \Psi}(l_2 C_{\theta_2} + l_3 C_{\theta_2 \theta_3}) & C_{\theta_1 \Psi}(l_2 C_{\theta_2} + l_3 C_{\theta_2 \theta_3}) & -S_{\theta_1 \Psi}(l_2 S_{\theta_2} + l_3 S_{\theta_2 \theta_3}) & -l_3 S_{\theta_1 \Psi} S_{\theta_2 \theta_3} \\ 0 & 0 & l_2 C_{\theta_2} + l_3 C_{\theta_2 \theta_3} & l_3 C_{\theta_2 \theta_3} \end{bmatrix}$$

Where $C_{\Psi}=\cos(\Psi)$ and $S_{\Psi}=\sin(\Psi)$; $C_{\theta_2}=\cos(\theta_2)$ and $S_{\theta_2}=\sin(\theta_2)$; $C_{\theta_1\Psi}=\cos(\theta_1+\Psi)$ and $S_{\theta_1\Psi}=\sin(\theta_1+\Psi)$; and $C_{\theta_2\theta_3}=\cos(\theta_2+\theta_3)$ and $S_{\theta_2\theta_3}=\sin(\theta_2+\theta_3)$.

Each row of J_{ee} corresponds to a Cartesian direction of the end-effector $(x_{ee}, y_{ee}, \text{ and } z_{ee})$, while each column is associated with one of the generalized velocities: u (linear), ω (angular), and $\dot{\theta}_1$, $\dot{\theta}_2$, $\dot{\theta}_3$ (joint velocities of the manipulator).

Given that the mass of the robotic arm is considerably smaller than that of the mobile platform, a kinematic model is used for the arm and a dynamic model for the mobile platform.

$$\begin{bmatrix} \dot{u} \\ \dot{\omega} \end{bmatrix} = \begin{bmatrix} \begin{pmatrix} \frac{B_3}{B_1} \end{pmatrix} \omega^2 - \begin{pmatrix} \frac{B_4}{B_1} \end{pmatrix} u \\ - \begin{pmatrix} \frac{B_5}{B_2} \end{pmatrix} u \omega - \begin{pmatrix} \frac{B_6}{B_2} \end{pmatrix} \omega \end{bmatrix} + \begin{bmatrix} \frac{1}{B_1} & 0 \\ 0 & \frac{1}{B_2} \end{bmatrix} \begin{bmatrix} u_r \\ \omega_r \end{bmatrix}$$

Where $[B] = [B_1, B_2, B_3, B_4, B_5, B_6]^T$ is the vector of identified parameters of the robot, u_r is the control input associated with the linear velocity of the mobile platform, and ω_r is the control input associated with its angular velocity.

The final model of the mobile manipulator is obtained by combining the kinematic model of the arm, presented in Eq. (7), with the dynamic model of the mobile platform, given in Eq. (9). This results in the complete representation summarized in Eq. (10).

$$\begin{bmatrix} \dot{x}_{ee} \\ \dot{y}_{ee} \\ \dot{z}_{ee} \\ \dot{\psi} \\ \dot{u} \\ \dot{\omega} \end{bmatrix} = \begin{bmatrix} uJ_{11} + \omega J_{12} + \dot{\theta}_{1}J_{13} + \dot{\theta}_{2}J_{14} + \dot{\theta}_{3}J_{15} \\ uJ_{21} + \omega J_{22} + \dot{\theta}_{1}J_{23} + \dot{\theta}_{2}J_{24} + \dot{\theta}_{3}J_{25} \\ uJ_{31} + \omega J_{32} + \dot{\theta}_{1}J_{33} + \dot{\theta}_{2}J_{34} + \dot{\theta}_{3}J_{35} \\ \omega \\ \left(\frac{B_{3}}{B_{1}}\right)\omega^{2} - \left(\frac{B_{4}}{B_{1}}\right)u + \frac{1}{B_{1}}u_{r} \\ - \left(\frac{B_{5}}{B_{2}}\right)u\omega - \left(\frac{B_{6}}{B_{2}}\right)\omega + \frac{1}{B_{2}}\omega_{r} \end{bmatrix}$$

$$(10)$$

where J_{mn} represents the elements of the Jacobian ma-

trix described in Eq. (8), which maps the generalized velocities to the Cartesian velocity of the end-effector.

3 DESIGN OF THE PROPOSED CONTROLLER

This section presents the development of the controllers. First, a sliding mode controller for the mobile manipulator is derived, and then the concept of a Clegg integrator is incorporated into its sliding surface.

3.1 Sliding Mode Controller for Mobile Manipulator

To compute the control inputs, the inverse kinematics of the mobile manipulator is calculated.

$$U = J_{\rho\rho}^+ \dot{h}_{\rho\rho} \tag{11}$$

Where $U = [u_c, \omega_c, \dot{\theta}_1, \dot{\theta}_2, \dot{\theta}_3]^T$ is the vector of control inputs generated through inverse kinematics, and J_{ee}^+ is the pseudoinverse of the Jacobian matrix J_{ee} , used to map the desired Cartesian velocity of the end-effector to the generalized control inputs. The pseudoinverse is computed using the Moore–Penrose formulation as:

$$J_{ee}^{+} = J_{ee}^{T} (J_{ee} J_{ee}^{T})^{-1}$$
 (12)

As described in the previous section, a sliding mode controller consists of a continuous component $U_{\rm C}$ and a discontinuous component $U_{\rm D}$. To compute the continuous component, a sliding surface must first be defined. In this work, a proportional-integral (PI) type surface is used:

$$s = e_h + \lambda_1 \int e_h \, dt \tag{13}$$

Where e_h is the tracking error, defined as the difference between the desired trajectory and the actual end-effector position, i.e., $e_h = h_d - h_{ee} =$ $[e_x, e_y, e_z]^T$; h_d represents the desired Cartesian trajectory of the end-effector; and λ_1 is a positive tuning parameter that determines the convergence rate of the sliding surface.

To satisfy the sliding condition, the derivative of the sliding surface must be equal to zero. Therefore, the time derivative of Eq. (13) is computed as:

$$\dot{s} = \dot{e}_h + \lambda_1 e_h = 0 \tag{14}$$

Since the tracking error is defined as $e_h = h_d - h_{ee}$, its time derivative is given by:

$$\dot{e}_h = \dot{h}_d - \dot{h}_{ee} \tag{15}$$

Substituting Eq. (15) into Eq. (14), the sliding surface derivative becomes:

$$\dot{s} = \dot{h}_d - \dot{h}_{ee} + \lambda_1 e_h = 0 \tag{16}$$

Solving for \dot{h}_{ee} yields:

$$\dot{h}_{ee} = \dot{h}_d + \lambda_1 e_h \tag{17}$$

Equation (17) provides the desired Cartesian velocity of the end-effector required to stay on the sliding surface. By substituting this expression into the inverse kinematics relation in Eq. (11), the continuous component of the sliding mode control law is obtained as:

$$U_{\rm C} = J_{ee}^+ \left(h_d + \lambda_1 e_h \right) \tag{18}$$

To obtain the discontinuous component of the controller, the Lyapunov stability concept is directly applied.

According to Lyapunov's direct method, if there exists a scalar function V, continuously differentiable and positive definite, such that its time derivative along the system trajectories \dot{V} is negative definite, then the equilibrium point at the origin is globally asymptotically stable.

Let $V = \frac{1}{2}s^T s$, which satisfies V > 0 for all $s \neq 0$, since $s^T s$ represents the squared norm of the vector s. If s = 0, then V = 0, as the norm of the zero vector is zero. The time derivative of V is given by $\dot{V} =$ $\frac{1}{2}\left(\dot{s}^Ts + s^T\dot{s}\right) = s^T\dot{s}.$

The error derivative in Eq. (14) is decomposed as $\dot{e}_h = \dot{h}_d - \dot{h}_{ee}$. Then, using the expression from Eq. (7), \dot{h}_{ee} is replaced by $J_{ee}U$, and this substitution is used to rewrite the sliding surface derivative.

$$\dot{V} = s^T \left(\dot{h}_d - J_{ee}U + \lambda_1 e_h \right) \tag{19}$$

If U_{SMC} is considered as the sum of its continuous and discontinuous components, that is, $U_{SMC} = U_{C} +$

 $U_{\rm D}$, and the expression for $U_{\rm C}$ from Eq. (18) is used, the following is obtained:

$$\dot{V} = -s^T J_{ee} U_{\rm D} \tag{20}$$

To ensure that $\dot{V} < 0$, the discontinuous component is defined as:

$$U_{\rm D} = J_{ee}^+ k_D \operatorname{sign}(s) \tag{21}$$

where k_D is a positive scalar or diagonal gain matrix that adjusts the intensity of the switching action. The matrix J_{ee}^+ denotes the pseudoinverse of the Jacobian matrix J_{ee} , and is used to project the control action from Cartesian space back to the generalized coordinates of the system. This operation allows the generation of appropriate control inputs that achieve the desired behavior of the end-effector in task space.

However, using the sign(s) function may cause chattering and excessive effort in the actuators of the mobile manipulator. Therefore, a smoothed version is used instead:

$$U_{\rm D} = J_{ee}^{+} \frac{k_D s}{\|s\| + \delta}$$
 (22)

where δ is a small positive scalar that smooths the discontinuity and reduces chattering effects. A larger value of δ increases the smoothness of the control signal but compromises the speed at which the system reaches the reference.

Replacing the smoothed expression of U_D into the derivative of the Lyapunov function yields:

$$U_{\rm C} = J_{ee}^{+} \left(\dot{h}_d + \lambda_1 e_h \right)$$
 (18)
$$\dot{V} = -s^T J_{ee} J_{ee}^{+} \frac{k_D s}{\|s\| + \delta}$$
 (23)

Assuming that $J_{ee}J_{ee}^{+}\approx I$, this simplifies to:

$$\dot{V} = -k_D \frac{s^T s}{\|s\| + \delta} \tag{24}$$

Since $k_D > 0$, it follows that $\dot{V} < 0$, which implies that $s \to 0$ as $t \to \infty$. From (13), and by introducing the change of variable $\rho = \int e_h dt$, we obtain:

$$0 = \dot{\rho} + \lambda_1 \rho \tag{25}$$

In order for the system solutionisfy $\rho \to 0$, it is required that $\lambda_1 > 0$. Consequently, $\rho = \int e_h dt \to 0$, which implies that $e_h \to 0$ as $t \to \infty$.

The complete control law can be expressed in a compact form as:

$$U_{\text{SMC}} = J_{ee}^{+} \left(\dot{h}_d + \lambda_1 e_h + \frac{k_D s}{\|s\| + \delta} \right)$$
 (26)

Sliding Mode Control Proposal with a Clegg Integrator

The approach proposed in this work uses a Clegg integrator in the sliding surface. Figure 2 presents a block diagram of the overall control strategy, which will be detailed in the following sections.

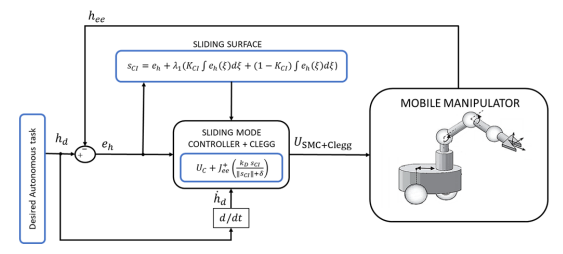


Figure 2: SMC+Clegg control scheme.

The resulting sliding surface, incorporating a Clegg integrator, is expressed as:

$$s_{\text{Cl}} = e_h + \lambda_1 \left(K_{\text{Cl}} \int_0^t e_h(\xi) d\xi + (1 - K_{\text{Cl}}) \int_{t_r}^t e_h(\xi) d\xi \right)$$
(27)

Where K_{Cl} is a scalar gain that determines the contribution of the Clegg integrator in the sliding surface. It must be bounded in the range $0 \le K_{Cl} \le 1$, where $K_{\rm Cl} = 1$ corresponds to a full Clegg integrator and $K_{\rm Cl} = 0$ to a conventional integrator. The variable ξ is used as the integration variable to avoid confusion with the upper limit t, and represents the intermediate time over which the error signal is integrated. The reset time t_r is updated whenever the derivative of the tracking error \dot{e}_h crosses zero; this mechanism eliminates the accumulation of past control actions and resets the integrator, thereby reducing windup effects. To avoid spurious resets caused by high-frequency noise, a moving average filter with a window of five sampling intervals was applied to \dot{e}_h prior to evaluating the reset condition.

Since the continuous component was obtained based on the sliding condition, which requires the time derivative of the sliding surface to be zero, the Clegg integrator has no effect on the continuous part of the controller. This is because the integral term in the sliding surface expression disappears when differentiating. As a result, the continuous component of a conventional SMC controller and that of the SMC+Clegg controller are the same. Therefore, the stability analysis of the continuous part presented in the previous section also applies to the proposed controller.

However, the discontinuous component of the controller directly depends on the sliding surface expression, which includes the Clegg integrator. Therefore, the effects of the Clegg integrator have a direct impact on the discontinuous control action, influence-

ing both the chattering behavior of the system and its settling time.

The complete control law, using the Clegg-integrated sliding surface, is defined as:

$$U_{\text{SMC+Clegg}} = J_{ee}^{+} \left(\dot{h}_d + \lambda_1 e_h + \frac{k_D s_{\text{Cl}}}{\|s_{\text{Cl}}\| + \delta} \right) \quad (28)$$

The simulation parameters used for the model and controller are as follows: the manipulator link lengths are $l_1=0.4$ m, $l_2=0.25$ m, and $l_3=0.25$ m; the vertical offset is $l_m=0.2$ m; the distances a and b are both set to 0.13 m. The dynamic coefficients used in the model are $B_1=0.2604$, $B_2=0.2509$, $B_3=-4.99\times 10^{-4}$, $B_4=0.9965$, $B_5=0.00263$, and $B_6=1.0768$. The control parameters include a sliding surface slope $\lambda_1=28$, Clegg integrator reset proportion $K_{Cl}=0.5$, smoothing parameter $\delta=0.8$, and sliding mode gain $k_D=11.5$.

4 RESULTS AND DISCUSSION

This section presents the results of the tests performed. A single experiment was conducted, consisting of trajectory tracking combined with an external disturbance to evaluate the performance of the conventional SMC controller and the proposed SMC+Clegg approach. The selected trajectory is an inclined-square path that includes sharp corners and sudden reference changes, designed to assess the controllers' performance under abrupt directional transitions and varying orientations.

As shown in Figure 3, the results of the tracking for the inclined-square trajectory are presented. The reference trajectory is shown in red, the response using the conventional SMC controller is shown in blue, and the response of the proposed SMC+Clegg integrator in the sliding surface is shown in black.

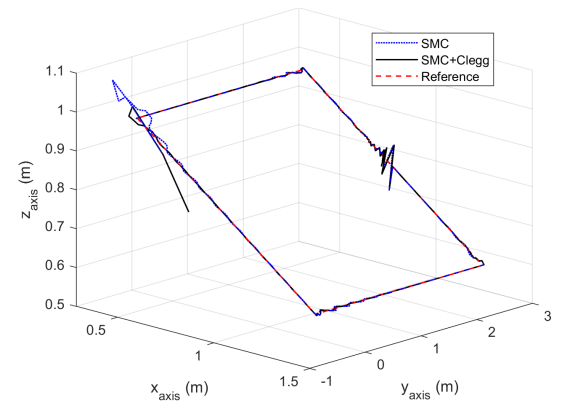


Figure 3: Tracking results for the inclined-square trajectory.

Figure 4 presents the tracking errors along the three Cartesian axes for the inclined-square trajectory. The effects of the disturbance introduced into the system at t = 15 s can also be observed in the responses.

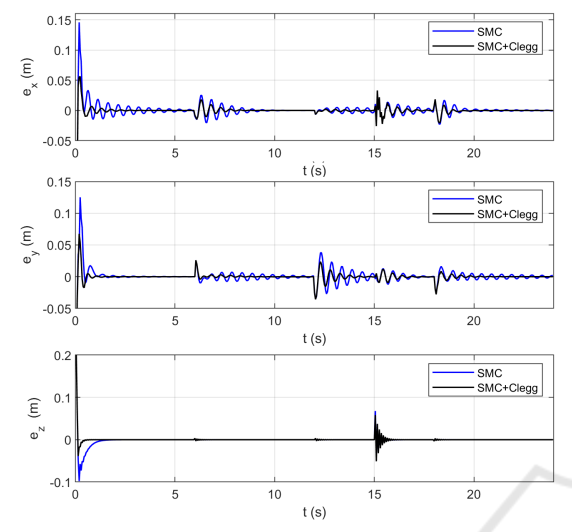


Figure 4: Tracking errors for the inclined-square trajectory. Top: error in the *x*-axis; middle: error in the *y*-axis; bottom: error in the *z*-axis.

As observed in the Figure 4, the introduction of the Clegg integrator in the sliding surface reduces both the amplitude and duration of the oscillations. The proposed approach improves the system's response in terms of trajectory tracking and recovery after disturbances in the inclined-square trajectory.

To highlight the impact of the proposed method on the control action, Figure 5 shows the norm of the control output vectors, with the conventional SMC controller in blue and the SMC+Clegg controller in black.

The greatest influence of the Clegg integrator occurs in the sliding surface, which is directly associated with the discontinuous component of the control law. As shown in Figure 5(a), the norm of U_D is significantly reduced when using the SMC+Clegg controller, indicating a more moderate control effort during transients. This reduction is more clearly observed in the zoomed view in Figure 5(b), where sharp variations are effectively attenuated. Figures 5(c) and 5(d) present the norm of the total control signal and its zoomed view, respectively, showing that the benefits of the proposed strategy extend to the overall control action, particularly during abrupt changes in the reference or in the presence of disturbances.

It is important to clarify that, although the discontinuous term is bounded due to the smoothing parameter applied to the switching function, the integral term in the sliding surface may still accumulate error during persistent transients. This accumulation can delay convergence and intensify the control action before correction occurs. By resetting the integral component whenever the error derivative crosses zero, the Clegg integrator mitigates this form of windup in the sliding surface, contributing to faster recovery and improved control smoothness during abrupt transitions.

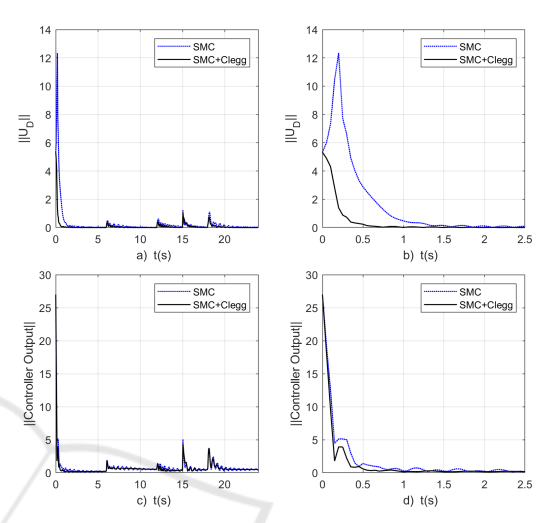


Figure 5: Norm of the controller vector: (a) discontinuous component U_D , (b) zoomed view of U_D , (c) total control signal, and (d) zoomed view of the total control signal.

Likewise, Figure 5(d) shows that noticeable differences between both controllers emerge primarily during abrupt reference changes or in the presence of disturbances. This behavior aligns with expectations, since the discontinuous component—where the Clegg integrator is applied—is activated mainly under significant tracking errors. During steady-state operation, when the system remains close to the reference, the control action is dominated by the continuous component, leading to similar behavior for both controllers.

To evaluate the performance of the controller, three standard indices were used: the Integral Square Error (ISE), the Integral Absolute Error (IAE), and the Total Variation of the control signal (TVu). These metrics were applied to quantify the tracking accuracy and control effort of each controller. Table 1 summarizes the results obtained for both controllers, including the percentage improvement achieved by the proposed SMC+Clegg controller relative to the conventional SMC controller. Additionally, since the Clegg integrator is applied in the discontinuous part of the control law, the TVu was also computed specifically for that component to assess its isolated effect on control smoothness.

Table 1: Performance comparison for the inclined-square trajectory.

Metric	SMC	SMC+Clegg	Δ (%)
IAE	0.21846	0.12332	43.55
ISE	0.01685	0.01377	18.30
TVu	7.51519	6.52225	13.21
$TVu\left(U_{D}\right)$	2.39366	1.40371	41.36

As evidenced by the results, the proposed SMC+Clegg controller achieved notable improvements in all performance indices. The IAE was reduced by over 43%, and the total variation of the discontinuous control signal (U_D) decreased by more than 41%, indicating a smoother and more efficient control effort. Although the reduction in ISE and overall TVu was more moderate, improvements of 18% and 13%, respectively, still reflect enhanced tracking precision and reduced control aggressiveness. Importantly, resetting the integral component did not compromise the system's ability to reject disturbances. In this study, a reset proportion of 50% $(K_{Cl} = 0.5)$ was employed, balancing convergence speed with control signal smoothness. This value was selected empirically based on iterative testing, as it provided a satisfactory trade-off between responsiveness and chattering attenuation. Nonetheless, systematic tuning or optimization of K_{Cl} may further improve performance and is considered for future work.

5 CONCLUSIONS

This work presented a sliding mode control strategy that incorporates a Clegg integrator into the sliding surface. The controller was implemented on a mobile manipulator combining the kinematic model of the arm and the dynamic model of the platform.

The system was evaluated using an inclined-square trajectory and external disturbances to test robustness. Compared to the conventional SMC, the proposed controller showed improved performance, with reduced overshoot duration and oscillations, smoother control signals, and effective mitigation of chattering. These improvements were reflected in the IAE, ISE, and TVu indices.

Stability is formally ensured via Lyapunov's direct method. The Clegg integrator only affects the discontinuous part of the control law, which is active mainly during transient phases, leaving the continuous component stable during steady-state.

Future work may include experimental validation and extension to systems with higher complexity or nonlinearities. It should be noted that the current results are limited to simulation only. Therefore, practical aspects such as sensor noise, actuator saturation, and discretization effects must be considered in future implementations, as they may affect the reset behavior and control smoothness.

Additionally, this work focused exclusively on the Clegg integrator due to its simplicity and proven effectiveness. A comparative analysis with other reset strategies—such as First-Order Reset Elements (FORE) or Generalized Reset Elements (GFORE)—was not conducted and remains an important direction for future research. Nonetheless, the proposed strategy relies on standard Jacobian inversion and integrator modification, which facilitates its application in embedded systems with typical sensing and actuation capabilities.

Moreover, extensions of sliding mode control such as higher-order sliding mode (HOSMC) and homogeneity-based designs were not considered in this study. These approaches offer improved convergence properties and enhanced robustness, and their integration with reset-based strategies could further improve system performance, representing a valuable direction for future exploration.

REFERENCES

- Beerens, R., Bisoffi, A., Zaccarian, L., Nijmeijer, H., Heemels, M., and van de Wouw, N. (2022). Reset pid design for motion systems with stribeck friction. *IEEE Transactions on Control Systems Technology*, 30(1):294–301.
- Chaudhary, B. (2024). Anti-windup strategy for interval positive linear systems with input saturation. *International Journal of Dynamics and Control*, 12:2842–2849.
- Delgado, M., Morales, R., García, J., and Pérez, L. (2022). Motion planning for mobile manipulators—a systematic review. *Machines*, 10(2):97.
- Demim, F., Rouigueb, A., Belaidi, H., Messaoui, A. Z., Bensseghieur, K. L., Allam, A., Benatia, M. A., Nouri, A., and Nemra, A. (2023). Smooth sliding mode control based technique of an autonomous underwater vehicle based localization using obstacle avoidance strategy. In Proceedings of the 20th International Conference on Informatics in Control, Automation and Robotics (ICINCO 2023), pages 529– 537. SCITEPRESS – Science and Technology Publications.
- Gan, D., Fu, J., Lin, H., Yang, H., Rastgaar, M., Min, B.-C., and Voyles, R. (2022). Actuation-coordinated mobile parallel robots with hybrid mobile and manipulation functions. *Journal of Mechanisms and Robotics*, 14(4):041005.
- Gholipour, E., Aref, M. M., and Fateh, M. M. (2015). 2-dof pid with reset controller for 4-dof robot arm manipulator. In 2015 3rd RSI International Conference on

- Robotics and Mechatronics (ICRoM), pages 704–709. IEEE
- Gude, J. J., Di Teodoro, A., Agudelo, D., Herrera, M., Rincón, L., and Camacho, O. (2024). Sliding mode control design using a generalized reduced-order fractional model for chemical processes. *Results in Engineering*, 24:103032.
- Haddadin, S., Albu-Schäffer, A., and Hirzinger, G. (2022). A holistic approach to reactive mobile manipulation. *IEEE Transactions on Robotics*, 38(1):3–22.
- Hitit, Z. Y., İsmet Koçer, Kuş, G., Arslan, N. Z., Dal, E. P., and Koz, H. (2023). Optimal pid control with anti-windup in neutralization process. *Interna*tional Advanced Researches and Engineering Journal, 7(3):138–145.
- Kemp, C. C., Edsinger, A., Clever, H. M., and Matulevich, B. (2022). The design of stretch: A compact, lightweight mobile manipulator for indoor human environments. In 2022 International Conference on Robotics and Automation (ICRA), pages 3150–3157.
- Kolar, A. and Lazar, M. (2021). Anti windup pid control of discrete systems subject to actuator saturation. In 2021 60th IEEE Conference on Decision and Control (CDC), pages 5104–5109, Austin, TX, USA. IEEE.
- Le, J. H. and Teel, A. R. (2021). Passive soft-reset controllers for nonlinear systems. In 2021 60th IEEE Conference on Decision and Control (CDC), pages 5320–5325.
- Li, X., Wang, Y., Liu, Y., Liu, Y., and Liu, Y. (2024). A novel hybrid control strategy for a class of nonlinear systems with input saturation. *Heliyon*, 10(9):e2590.
- Maung, L. M. M., San, A. M., Myint, W. M., Win, W. Y., and Soe, M. T. (2024). Analysis of the pid controller parameters for a surface mobility platform mobile robot. *PLATFORM A Journal of Engineering*, 8(2):29–40. Creative Commons CC BY 4.0.
- Moreno, G. P., la Cruz, N. D. D., Ortiz, J. S., and Andaluz, V. H. (2021). Human-robot collaborative control for handling and transfer objects. In *Applied Technolo*gies, volume 1388 of *Communications in Computer* and Information Science, pages 96–110. Springer.
- Okelola, M. O., Aborisade, D. O., and Adewuyi, P. A. (2020). Performance and configuration analysis of tracking time antiwindup pid controllers. *Jurnal Ilmiah Teknik Elektro Komputer dan Informatika* (*JITEKI*), 6(2):20–29.
- Proaño, P., Díaz, R., Chillán, C., Medina, J., Chamorro, W., and Zuñiga, J. (2024). Sliding mode control proposed using a clegg integrator for speed control of a three-phase induction motor. In *Proceedings of the XXXII Conference on Electrical and Electronic Engineering*, volume 77, page 8. MDPI.
- Salinas, L. R., Santiago, D., Slawiñski, E., Mut, V. A., Chavez, D., Leica, P., and Camacho, O. (2018). P+d plus sliding mode control for bilateral teleoperation of a mobile robot. *International Journal of Control, Au*tomation and Systems, 16(4):1927–1937.
- Teel, A. R. (2022). Continuous-Time Implementation of Reset Control Systems, pages 27–41. Springer International Publishing, Cham.

- V, V. D. and Manthati, U. B. (2024). Advanced strategies for chattering reduction in sliding mode-controlled bidirectional cuk converters. In 2024 IEEE 1st International Conference on Green Industrial Electronics and Sustainable Technologies (GIEST), pages 1–5.
- Vizuete, R., Torres, J. A., and Leica, P. (2017). Trajectory tracking based on containment algorithm applied to a formation of mobile manipulators. In *Proceedings of the 14th International Conference on Informatics in Control, Automation and Robotics (ICINCO 2017), Volume 1*, pages 122–131.
- Widhiada, W., Santhiarsa, I. G. N., and Partha, C. G. I. (2020). Design of motion control for mobile robot manipulator. *International Journal of Mechanical En*gineering and Robotics Research, 9(11):1509–1514.
- Yim, J., You, S., Lee, Y., and Kim, W. (2023). Chattering attenuation disturbance observer for sliding mode control: Application to permanent magnet synchronous motors. *IEEE Transactions on Industrial Electronics*, 70(5):5161–5170.
- You, Y., Fan, Z., Chen, W., Zhu, G., Qiu, B., Xin, J., Chen, J., Deng, F., Hou, Y., Liang, W., and Fu, R. (2019). Design and implementation of mobile manipulator system. In 2019 IEEE 9th Annual International Conference on CYBER Technology in Automation, Control, and Intelligent Systems (CYBER), pages 113–118.
- Zangina, U., Buyamin, S., Abidin, M. S. Z., Mahmud, M. S. A., and Hasan, H. S. (2020). Non-linear pid controller for trajectory tracking of a differential drive mobile robot. *Journal of Mechanical Engineering Research and Developments*, 43(7):255–270. ISSN: 1024-1752, CODEN: JERDFO.
- Zhao, J., Giammarino, A., Lamon, E., Gandarias, J. M., Momi, E. D., and Ajoudani, A. (2022). A hybrid learning and optimization framework to achieve physically interactive tasks with mobile manipulators. *IEEE Robotics and Automation Letters*, 7(3):8036– 8043.